A comprehensive picture in the view of atomic scale on piezoelectricity of ZnO tunnel junctions: The first principles simulation

Genghong Zhang, Weijin Chen, Jia Zhu, Gelei Jiang, Qiang Sheng, Biao Wang, and Yue Zheng

Citation: AIP Advances **6**, 065217 (2016); doi: 10.1063/1.4954696
View online: https://doi.org/10.1063/1.4954696
View Table of Contents: http://aip.scitation.org/toc/adv/6/6
Published by the American Institute of Physics

Articles you may be interested in

Electromechanical scale-bridging model for piezoelectric nanostructures
Applied Physics Letters **110**, 013104 (2017); 10.1063/1.4973631

Ferroelectric or non-ferroelectric: Why so many materials exhibit "ferroelectricity" on the nanoscale
Applied Physics Reviews **4**, 021302 (2017); 10.1063/1.4979015

Theoretical study on the top- and enclosed-contacted single-layer MoS_2 piezotronic transistors
Applied Physics Letters **108**, 181603 (2016); 10.1063/1.4948660

Ab initio and experimental studies of polarization and polarization related fields in nitrides and nitride structures
AIP Advances **7**, 015027 (2017); 10.1063/1.4974249

Commentary: The Materials Project: A materials genome approach to accelerating materials innovation
APL Materials **1**, 011002 (2013); 10.1063/1.4812323

Fundamental study of mechanical energy harvesting using piezoelectric nanostructures
Journal of Applied Physics **108**, 034309 (2010); 10.1063/1.3462468

A comprehensive picture in the view of atomic scale on piezoelectricity of ZnO tunnel junctions: The first principles simulation

Genghong Zhang,[1,2] Weijin Chen,[1,2,3] Jia Zhu,[1,2] Gelei Jiang,[1,2] Qiang Sheng,[1,2] Biao Wang,[1,3,a] and Yue Zheng[1,2,b]
[1]*State Key Laboratory of Optoelectronic Materials and Technologies, School of Physics and Engineering, Sun Yat-sen University, Guangzhou 510275, China*
[2]*Micro&Nano Physics and Mechanics Research Laboratory, School of Physics and Engineering, Sun Yat-sen University, Guangzhou 510275, China*
[3]*Sino-French Institute of Nuclear Engineering and Technology, Sun Yat-Sen University, Zhuhai 519082, China*

(Received 24 December 2015; accepted 12 June 2016; published online 17 June 2016)

Piezoelectricity is closely related with the performance and application of piezoelectric devices. It is a crucial issue to understand its detailed fundamental for designing functional devices with more peculiar performances. Basing on the first principles simulations, the ZnO piezoelectric tunnel junction is taken as an example to systematically investigate its piezoelectricity (including the piezopotential energy, piezoelectric field, piezoelectric polarization and piezocharge) and explore their correlation. The comprehensive picture of the piezoelectricity in the ZnO tunnel junction is revealed at atomic scale and it is verified to be the intrinsic characteristic of ZnO barrier, independent of its terminated surface but dependent on its c axis orientation and the applied strain. In the case of the ZnO c axis pointing from right to left, an in-plane compressive strain will induce piezocharges (and a piezopotential energy drop) with positive and negative signs (negative and positive signs) emerging respectively at the left and right terminated surfaces of the ZnO barrier. Meanwhile a piezoelectric polarization (and a piezoelectric field) pointing from right to left (from left to right) are also induced throughout the ZnO barrier. All these piezoelectric physical quantities would reverse when the applied strain switches from compressive to tensile. This study provides an atomic level insight into the fundamental behavior of the piezoelectricity of the piezoelectric tunnel junction and should have very useful information for future designs of piezoelectric devices. © *2016 Author(s). All article content, except where otherwise noted, is licensed under a Creative Commons Attribution (CC BY) license (http://creativecommons.org/licenses/by/4.0/).*
[http://dx.doi.org/10.1063/1.4954696]

I. INTRODUCTION

Piezoelectricity, a well-known effect discovered as early as 1880, has received much attention in the past decades and various devices basing on piezoelectric effect have been exploited and show excellent performances.[1–4] The proverbial conventional piezoelectric material is the perovskite structured $Pb(Zr_{1-x}Ti_x)O_3$ (PZT) due to its high piezoelectric coefficient, which has been extensively used in piezoelectric sensors, actuators and energy generators.[3,5,6] However, PZT is mainly used in the ceramic field whereas less used in the electronic and optoelectronic fields since it is electric insulating. As a piezoelectric candidate using in electronic and optoelectronic functional

[a]Electronic mail: wangbiao@mail.sysu.edu.cn
[b]Author to whom correspondence should be addressed. Electronic mail: zhengy35@mail.sysu.edu.cn

 ©Author(s) 2016.

devices, the piezoelectric material should be electrically conductive. Recently, the promising candidates of piezoelectric materials to be used in electronic and optoelectronic fields have been focused on the piezoelectric semiconductor materials in the wurtzite oxide, nitride and sulfide, such as the ZnO, GaN and CdS, etc.[7–10] In particular, on the basis of profuse nanostructures,[11] and abundant unique characteristics[12] ZnO has been considered as the most excellent piezoelectric semiconductor material, which can be utilized to construct functional nanodevices. Nowadays, lots of novel ZnO nanodevices with extraordinary performances have been fabricated[7,13,14] and widely applied in the fields of electronics, piezotronics, optoelectronics and so on.[15–17]

The extraordinary performance and extensive application of the ZnO device are closely related to its piezoelectricity. Understanding the detailed fundamentals of ZnO's piezoelectricity and its impact is a crucial issue for innovatively designing and fabricating ZnO functional devices with more peculiar performances. There have been many investigations on this issue basing on the continuum model and semiempirical model using the finite element method and molecular dynamics method. For example, Wang et al.[18–20] have studied the piezoelectric potential (piezopotential) spatial distribution and its influence on the local contact dictated transport character in strained ZnO nanowires and established the fundamental theory of piezotronics basing on the continuum model and finite element method. The piezoelectrically induced electric polarization and the associated potential as well as the piezoelectric coefficients in ZnO nanowires were also studied by Sen et al.[21] and Hoang et al.[22] Basing on the semiempirical molecular dynamics, the piezoelectric constant and polarization of ZnO as well as their size effect and surface effect have also been investigated.[23–25] Besides, first principles simulations have also been employed to study the piezoelectricity of ZnO devices recently. On the basis of the first principles simulations, Zhang et al.[26] investigated the piezoelectric effect as well as the piezoresistance effect in strained ZnO tunnel junctions and revealed its giant piezoelectric resistance effect. Agrawal et al.[9] also researched the giant piezoelectric size effect in ZnO nanowires. More recently, the potential barrier and polarization in strained ZnO tunnel junctions as well as their size effects were also studied.[27] Meanwhile, it was reported that the atomic scale origin of piezoelectricity in the wurtzite ZnO is due to the asymmetric hybridization between the Zn $3d_z^2$-$4p_z$ self-mixed orbital and the O $2p_z$ orbital along the polar c axis.[28] Moreover, using the density function theory and Poisson equation, the strain dependent piezocharge distributions at Ag/ZnO interfaces have been investigated and the width of the piezocharge distribution at the local interface, which reputedly can not be provided by the classical piezotronic theory, has been obtained.[29]

It is well known that the first principles simulation is an important method for calculating electronic structures based entirely on quantum mechanics and basic physical constants without any artificial parameters. It can provide basic information to quantitatively understand the piezoelectricity at atomic scale. In spite of extensive studies on the ZnO's piezoelectricity, however, to the best of our knowledge, most of them focus on its sporadic piezoelectric properties and little literature has been done to report the comprehensive picture of its piezoelectricity, especially with the method of atomic scale first principles quantum theory. Although there has been a general impression on the piezoelectricity of ZnO devices (strain will result in piezocharge, piezopotential, piezoelectric field and even piezoelectric polarization in ZnO devices), it is still of great significance to clearly reveal the comprehensive picture of ZnO's piezoelectricity in the view of atomic scale and explore the correlation between various piezoelectric physical quantities, which is important in quantitatively understanding the piezoelectric effect and guiding the innovative design of peculiar ZnO functional devices.

Accordingly, employing first principles quantum simulations, we take the ZnO piezoelectric tunnel junction as an example to systematically investigate its embedded piezoelectricity (including the piezopotential energy, piezoelectric field, piezoelectric polarization and the piezocharge) and explore their correlation. The comprehensive picture of the piezoelectricity in the ZnO tunnel junction is revealed at atomic scale and it is verified to be the intrinsic characteristic of ZnO barrier, independent of its terminated surface but dependent on its c axis orientation.

II. SIMULATION DETAILS

The following simulations are based on the density functional theory (DFT) within the generalized gradient approximation with Perdew-Burke-Ernzerhof parameterization (GGA.PBE)[30] performed in Vienna *ab initio* simulation package (VASP).[31,32] A plane wave basis set with 500 eV energy cutoff based on the projector-augmented wave method (PAW)[33] is used for the calculation. A $9 \times 9 \times 3$ k-point mesh in the Brillouin zone based on the Monkhorst-Pack method[34] are used for the structure optimized relaxation. Meanwhile, the energy convergence criterion is set to 0.01 meV. To obtain accurate calculation results, the k-point mesh is increased to $13 \times 13 \times 3$ for the self-consistent calculation.

The simulated piezoelectric tunnel junction is schematically shown in Fig. 1(a). It is constructed by a piezoelectric barrier sandwiched with two electrodes. Due to its non centrosymmetric structure, the piezoelectric barrier possesses two dissimilar terminated surfaces, which will result in a potential energy drop throughout itself and a subsequent built-in electric field as well as a spontaneous polarization. When an external strain is applied on it, the piezoelectric barrier will exhibit piezoelectric characteristic and result in a series of changes in the potential energy, built-in electric field, polarization and charge distribution. Here we will comprehensively investigate these changes and explore the embedded piezoelectricity at atomic scale. Meanwhile we will also verify its inherence (i.e., relevant with terminated surfaces or not).

To investigate the atomic scale microscopy piezoelectricity, the typical piezoelectric material ZnO and its tunnel junction Ag-ZnO-Ag are taken as examples. According to the crystal structure of ZnO as shown in Fig. 1(b), ZnO films possess two different terminated surface structures, labeled as the zigzag type ZnO film and the polar type ZnO film, respectively. Note that the separation energy to form these two kinds of ZnO films is different. However, in order to compare, explore, verify and show the inherence of the hidden piezoelectricity more clearly, these two kinds of ZnO films are both taken to construct ZnO tunnel junctions, named as Ag-ZnO-Ag_zigzag and Ag-ZnO-Ag_polar respectively. The ZnO tunnel junctions are constructed by aligning the (0001) oriented ZnO films with the Ag (111) electrodes according to their atom stacking sequences. On the basis of the conventional treatment method, the unit cell lattice constants in the x-y plane of electrodes are set

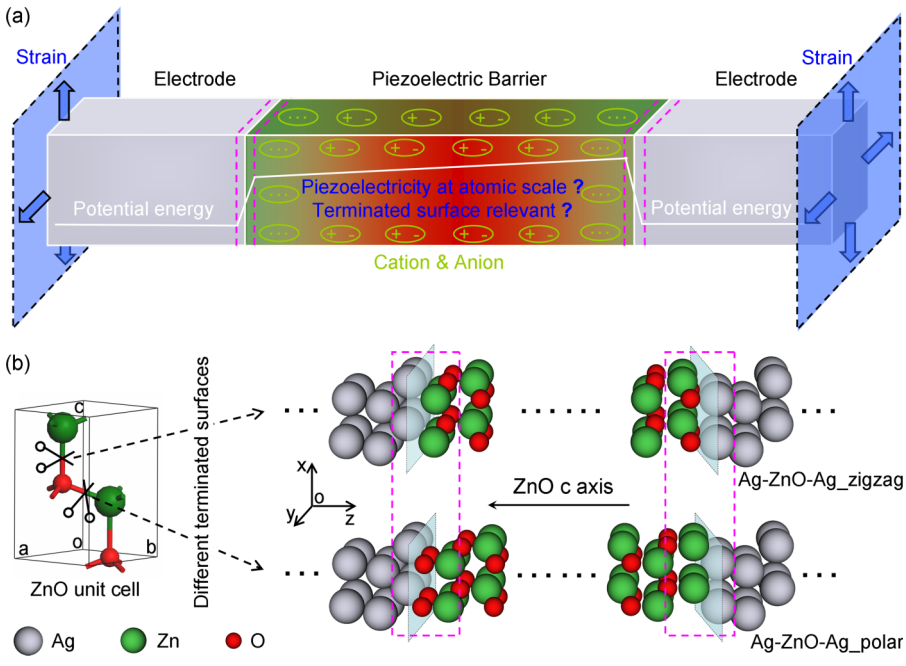

FIG. 1. (a) Schematic illustration of a piezoelectric tunnel junction under strain. Strain is applied along the in-plane lattice basic vectors. (b) Atomic structures of two ZnO piezoelectric tunnel junctions with different ZnO terminated surface structures whereas identical c axis orientation. The red dashed panes indicate the terminated and interfacial structures.

as those of the ZnO barrier.[35,36] Note that although the ZnO terminated surface structures in the two tunnel junctions are different, the c axis orientation of the central ZnO barrier is identical. It is pointing from the right electrode to the left electrode. The constructed tunnel junctions comprise 6 single Zn-O layers in the central barrier region sandwiched by 8 and 7 Ag layers as the left and right electrodes, respectively. It is periodically expanding in the x-y plane perpendicular to the c axis. The in-plane lattice constants of the constructed tunnel junction free of external strain are set as those of the bulk ZnO (~3.29 Å). Then external strain is applied in the system's x-y plane along the directions of the in-plane lattice basic vectors, as shown in Fig. 1(a). Strain is defined as $\eta = (a - a_0)/a_0$, where a and a_0 are the in-plane lattice constants of the tunnel junctions with and without strain respectively. Positive strain means tensile strain while negative strain is compressive strain. Positions of each atom and the out-of-plane lattice constant along z direction of the constructed ZnO tunnel junctions at each strain are fully relaxed.

III. RESULTS AND DISCUSSIONS

A. Structure based potential energy drop, built-in electric field, spontaneous polarization and charge distribution

It is well known that structure will affect and even determine properties. Due to the different ZnO terminated surface structures, electrical properties in the two ZnO tunnel junctions will exhibit distinct features. Figs. 2(a) and 2(c) depict the dissimilar electrostatic potential energies of electron in the two ZnO tunnel junctions free of external strain. The oscillatory black line and the smooth red line are the planar average (PA) potential energy and its smoothing curve (i.e., the double macroscopic average (DMA) potential energy).[37–39] It can be seen that there is a potential energy drop throughout the ZnO barrier due to the non centrosymmetric structure of ZnO, which is consistent with other report.[35] Furthermore, the potential energy drops in the two ZnO tunnel junctions are in opposite directions because of their different terminated surface structures. The

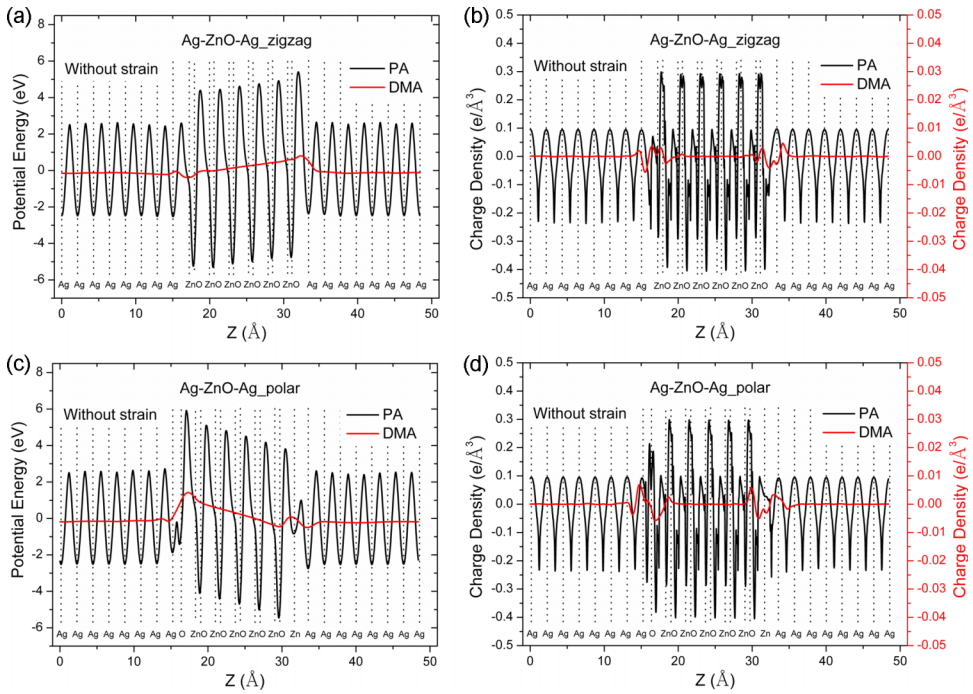

FIG. 2. Planar average (PA) electrostatic potential energy and charge density along z direction of the two ZnO tunnel junctions without strain. Their double macroscopic averages (DMAs) are also plotted (red lines). The dotted line labels the position of each atomic layer.

outmost atomic layers of the ZnO barrier in the left and right interfaces are Zn and O layers respectively in the Ag-ZnO-Ag_zigzag tunnel junction whereas they are O and Zn layers respectively in the Ag-ZnO-Ag_polar tunnel junction. It is known that the electric potential of the cation (Zn) is positive whereas it is negative for the anion (O). Thus the potential energy of electron in the Zn terminated surface is lower than that in the O terminated surface. Therefore the potential energy of the ZnO barrier increases along the z direction in the Ag-ZnO-Ag_zigzag tunnel junction whereas decreases in the Ag-ZnO-Ag_polar tunnel junction. The potential energy drop implies a built-in electric field in the ZnO barrier. By linear fitting the DMA energy drop of the central ZnO barrier, we can estimate the opposite built-in electric fields in the Ag-ZnO-Ag_zigzag and Ag-ZnO-Ag_polar tunnel junctions to be about 0.52 V/nm and −1.21 V/nm, respectively. Here the direction of positive electric field is pointing from the left electrode to the right electrode, i.e., the opposite direction of the ZnO c axis.

In the wurtzite ZnO, each ion (Zn or O) is tetrahedrally coordinated with four other type ions (O or Zn), forming a tetrahedral unit. However, due to the non centrosymmetry of ZnO, the center of the positive charge is displaced with respect to that of the negative charge along the c axis, which results in a spontaneous polarization in the ZnO barrier free of external strain. By calculating the atomic Born effective charges of ZnO using density functional perturbation theory (DFPT)[40,41] and then multiplied by the relative displacement along z direction between the cation and anion in every ZnO tetrahedron per unit volume, the average spontaneous polarizations of the ZnO barriers in the Ag-ZnO-Ag_zigzag and Ag-Zno-Ag_polar tunnel junctions free of external strain are estimated to be 0.073 C/m^2 and −0.039 C/m^2, respectively. It is worth noting that since the DFPT implemented in VASP is not suitable for metallic systems (ZnO barrier with metallic electrodes), the atomic Born effective charge of ZnO barrier under each strain is obtained from its bulk material with corresponding strain. Here the positive direction of the polarization is also pointing from the left electrode to the right electrode, i.e., the opposite direction of the ZnO c axis. We can see that although the spontaneous polarizations (0.073 C/m^2 and −0.039 C/m^2) as well as the built-in electric fields (0.52 V/nm and −1.21 V/nm) in the Ag-ZnO-Ag_zigzag and Ag-ZnO-Ag_polar tunnel junctions free of external strain are in opposite directions, the direction of the spontaneous polarization is identical with that of the built-in electric field in each ZnO tunnel junction.

By applying the Poisson's equation,[29] the planar average charge density distributions along z direction in the two ZnO tunnel junctions free of external strain can be derived from the planar average electrostatic potential energies, which are shown as the black lines in Figs. 2(b) and 2(d). Meanwhile, their double macroscopic averages (DMAs) are also plotted as the red lines. Here the electron potential energy and subsequent charge density comprise the contributions from the ionic potential and the electron Hartree potential. It can be seen that the charge densities in the inner Ag electrode and the inner ZnO barrier are flat and the total charge amount is zero since the ZnO systems are electrically neutral.[29] However, in the interface regions, we can see an obvious charge transfer and accumulation due to the interaction between the ZnO barrier and the electrode.

In both ZnO tunnel junctions, we can see that there are distinct distortions nearby interfaces in both potential energy and charge density as a result of the interface effect. Furthermore, due to the non centrosymmetric structure of ZnO, the left and right terminated surfaces of ZnO barrier is dissimilar, which results in the consistent potential energy drop, built-in electric field and spontaneous polarization in each tunnel junction. In addition, the directions of these electrical properties in Ag-ZnO-Ag_zigzag and Ag-ZnO-Ag_polar tunnel junctions are respectively opposite since the terminated surface structures in these two tunnel junctions are different. So all these electrical properties of the two ZnO tunnel junctions free of external strain are induced based on structure.

B. Strain induced piezopotential energy and piezoelectric field

Besides the influence factor of structure, strain should also play an important role in the ZnO tunnel junction since the ZnO barrier is piezoelectric. To investigate the impact of strain and explore the embedded piezoelectric behavior, strain dependent electrostatic potential energy is studies. The DMAs of potential energy in the inner ZnO region for the two ZnO tunnel junctions under strain are shown in Fig. 3. Here the potential energy at the center of the ZnO barrier is set as the referenced

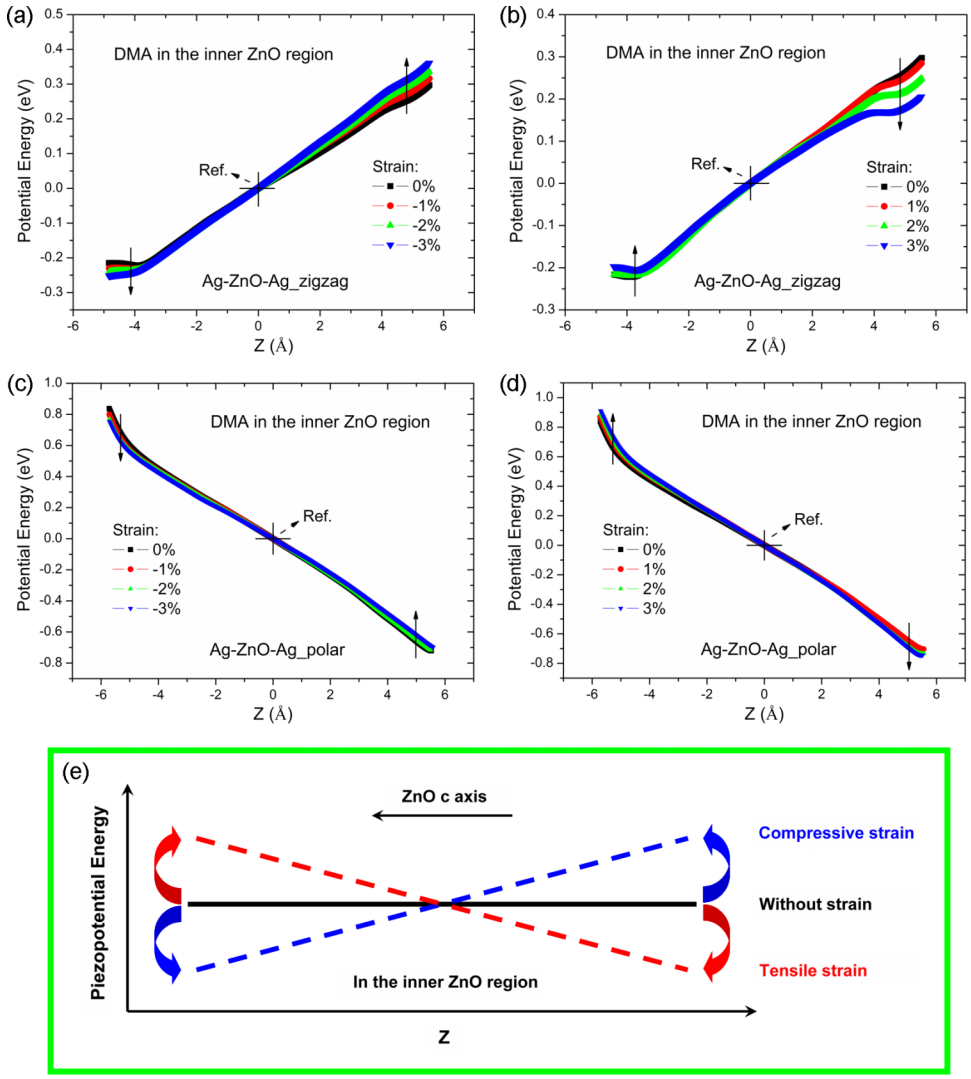

FIG. 3. (a)~(d) Double macroscopic average (DMA) of electrostatic potential energy in the inner ZnO region for the two ZnO tunnel junctions under strain. (e) The derived piezopotential energy profile of the ZnO barrier, which is the intrinsic characteristic of ZnO barrier, independent of its terminated surface but dependent on its c axis orientation.

zero-point energy. It can be seen that strain can adjust the potential energy drop of the ZnO barrier. In the Ag-ZnO-Ag_zigzag tunnel junction, the potential energy near the left interface decreases and that near the right interface rises with the increasing compressive strain. As a result, the potential energy drop gets steeper and steeper under compressive strain. When a tensile strain is applied, the slope of the potential energy drop gradually flattens. However, the evolution trend of the potential energy drop in the Ag-ZnO-Ag_polar tunnel junction is reverse. The potential energy drop in the Ag-ZnO-Ag_polar tunnel junction gradually flattens under compressive strain whereas it gets gradually steeper under tensile strain.

The variation of potential energy with strain implies a strain induce reversible piezopotential energy in the ZnO barrier. To explore the hidden piezopotential energy from above strain dependent potential energies, one needs to lay flat the potential energy of the ZnO barrier without strain to eliminate the structure based potential energy. After laying flat the DMA potential energies of ZnO barriers in the two tunnel junctions without strain, the embedded strain induced piezopotential energy is shown in Fig. 3(e). It is found that the piezopotential energy is followed by both the Ag-ZnO-Ag_zigzag and Ag-ZnO-Ag_polar tunnel junctions since their ZnO c axis orientations are

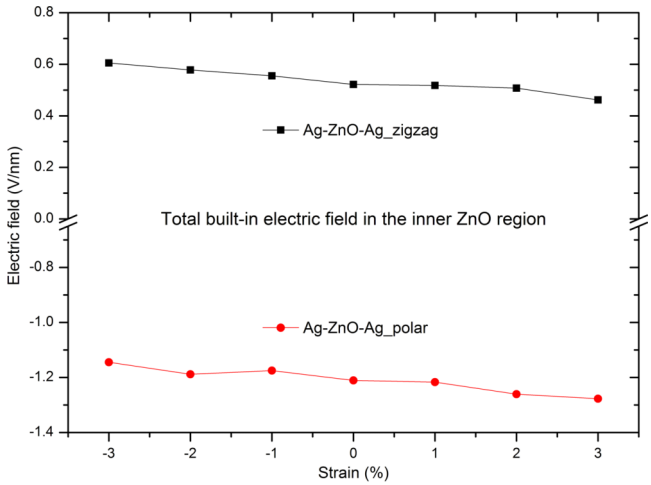

FIG. 4. Dependence of the total built-in electric field in the inner ZnO region of the two ZnO tunnel junctions on strain.

identical. In the case of the c axis of ZnO barrier pointing from right to left, a negative piezopotential energy in the left terminated surface of ZnO barrier will emerge whereas a positive piezopotential energy will emerge in the right ZnO terminated surface when a compressive strain is applied. The piezopotential energy distribution throughout the ZnO barrier will be reversed after applying a tensile strain. The magnitude of the piezopotential energy increases with the increasing strain. Note that this derived piezopotential energy is the intrinsic characteristic of ZnO barrier and is independent of the terminated surface structure but dependent on the c axis orientation of ZnO. The calculated potential energy within the ZnO barrier under strain as shown in Fig. 3 is comprised by the dissimilar terminated surfaces induced structural potential energy and the reversible strain dependent piezopotential energy. The opposite evolution trend of the potential energy drop in the two ZnO tunnel junctions under strain is resulted from the inverse structure based initial potential energy.

The strain induced reversible piezopotential energy also implies a reversible strain dependent piezoelectric field, which is coupling with the structure based electric field and then forms the total built-in electric field as shown in Fig. 4. The total built-in electric fields of the strained Ag-ZnO-Ag_zigzag and Ag-ZnO-Ag_polar tunnel junctions are positive and negative respectively, which are the same as their structure based electric fields without strain. It implies that strain adjusts the built-in electric field on the basis of the structure based electric field. The total built-in electric field in the Ag-ZnO-Ag_zigzag tunnel junction increases with the increasing compressive strain and decreases with the increasing tensile strain. On the other hand, in the Ag-ZnO-Ag_polar tunnel junction, the total built-in electric field decreases under compressive strain and increases under tensile strain. This reverse evolution trend is due to the opposite structure based built-in electric fields of the two ZnO tunnel junctions free of external strain. Meanwhile, it also implies the structure independent piezoelectric field in the ZnO barrier under strain. For both two ZnO tunnel junctions, after filtering out the structure based built-in electric field, we can find that a positive piezoelectric field (in the opposite direction of the ZnO c axis) will emerge in the ZnO barrier under compressive strain whereas a negative piezoelectric field will be induced under tensile strain. This piezoelectric field is an intrinsic characteristic of ZnO barrier and dependent on the applied strain as well as the ZnO c axis orientation.

C. Strain dependent piezoelectric polarization in the ZnO barrier

Hereinabove, we have seen that there is a spontaneous polarization in the ZnO barrier due to the misalignment between the centers of the positive charge and negative charge in the ZnO tetrahedral unit. Besides the structure induced spontaneous polarization, the total average polarizations of ZnO barriers in the Ag-ZnO-Ag_zigzag and Ag-ZnO-Ag_polar tunnel junctions under strain are also shown in Figs. 5(a) and 5(b), respectively. It can be seen that the total polarization is linearly

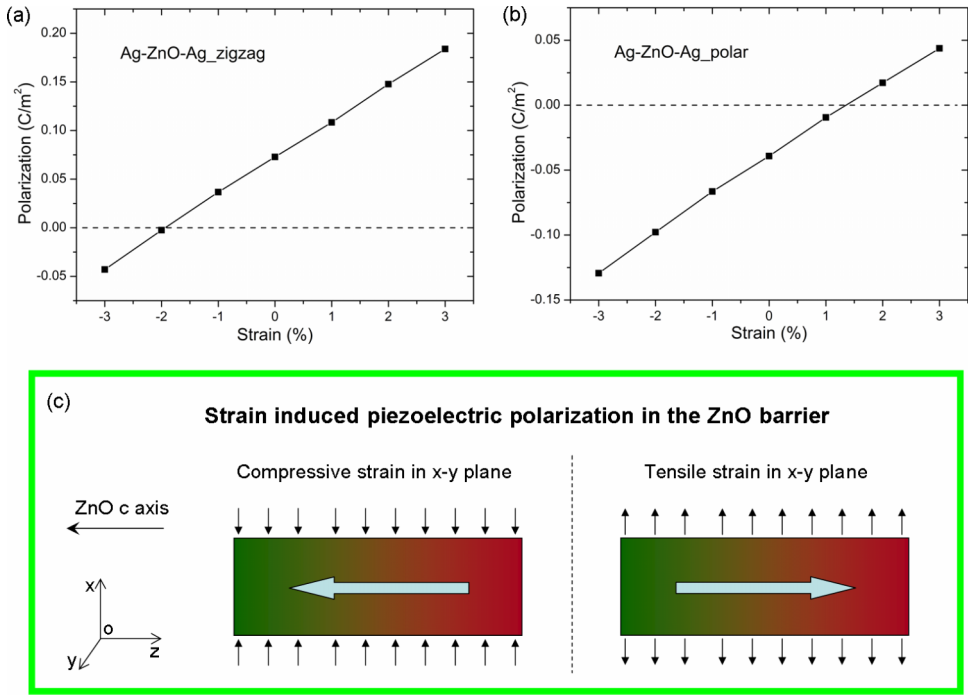

FIG. 5. Total average polarization of ZnO barrier in the two ZnO tunnel junctions under strain and the derived strain induced piezoelectric polarization profile of the ZnO barrier.

dependent on the applied strain, which is also reported in ZnO nanowires.[42] In the Ag-ZnO-Ag_zigzag tunnel junction, the total polarization is enhanced under tensile strain whereas it will be weaken and even reversed under compressive strain, which is consistent with experimental results.[27] The spontaneous polarization is almost counteracted under the compressive strain of −2%. On the other hand, in the Ag-ZnO-Ag_polar tunnel junction, the total polarization exhibits a distinct behavior. It is enhanced with the increasing compressive strain whereas weaken and even reversed with the increasing tensile strain. A tensile strain of about 1% should be applied to counteract the spontaneous polarization in the Ag-ZnO-Ag_polar tunnel junction. Similarly, this opposite evolution trend of the total polarizations in the two ZnO tunnel junctions should be due to their reverse structure based spontaneous polarizations.

The above total polarization under strain is actually composed of the structure based spontaneous polarization and the strain induced piezoelectric polarization. The piezoelectric polarization can be defined as the difference of polarization in the tunnel junctions with and without applied strain. Thus basing on Figs. 5(a) and 5(b), the strain induced piezoelectric polarization profile can be derived and is shown in Fig. 5(c). It is found that the piezoelectric polarization is also followed by both the ZnO tunnel junctions. In the case of the c axis of ZnO barrier pointing from right to left, a piezoelectric polarization pointing from right to left will be induced in the ZnO barrier after applying an in-plane compressive strain to the barrier. The induced piezoelectric polarization in the ZnO barrier can be reversed by switching the applied strain from compressive to tensile. Meanwhile, the magnitude of the piezoelectric polarization increases with the increasing strain. This reversible piezoelectric polarization is also the intrinsic characteristic of ZnO barrier and is independent of the terminated surface structure but dependent on the c axis orientation of ZnO barrier. We have to note that, hereinabove, the direction of the structure based spontaneous polarization in each ZnO tunnel junction free of external strain is identical with that of the structure based built-in electric field. However, from the comparison of the piezoelectric polarization and the piezoelectric field, we can find that the piezoelectric polarization and the piezoelectric field under identical strain are in opposite directions. Actually, the strain induced piezoelectric field is associated with the depolarization field, which will resist the piezoelectric polarization.

D. Strain induced piezocharge in the ZnO barrier

For a piezoelectric tunnel junction under strain, the piezocharge is an important factor and all other piezoelectric physical quantities (including the piezopotential, piezoelectric field and piezoelectric polarization, etc.) are associated with the pirzocharge distribution. According to the classical piezoelectric theory, the strain induced piezocharge can be defined as the charge difference between the devices with and without strain. The piezocharge density distribution of ZnO barrier in the two ZnO tunnel junctions under different strains is shown in Fig. 6. The position of each atomic layer is labeled by the dotted line. From this atomic scale piezocharge density distribution, we can clearly see the distinct piezoelectric effect. The strain dependent piezoelectric effect exits not only

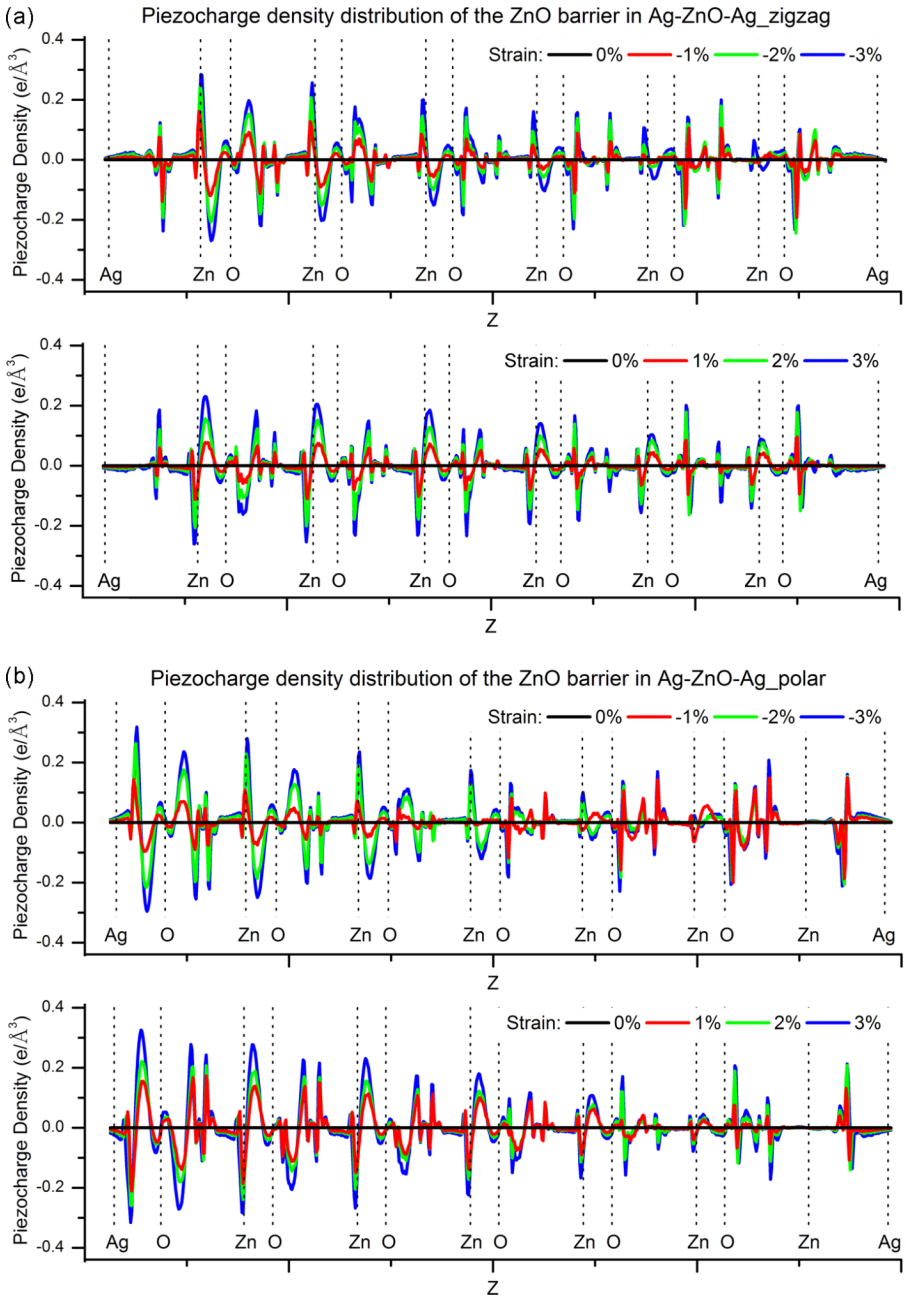

FIG. 6. Piezocharge density distribution of ZnO barrier in the two ZnO tunnel junctions under strain. The position of each atomic layer is labeled by the dotted line.

in the interface regions but also in the inner ZnO region. The calculated piezocharge distribution is abrupt and shows obvious atomic scale fluctuation.[29] It can be seen that the applied strain does not obviously affect the structure of the piezocharge density distribution but will change its magnitude. In the Ag-ZnO-Ag_zigzag tunnel junction, the piezocharge density increases with the increasing compressive strain. When the applied strain switches from compressive to tensile, the sign of the piezocharge density is also reversed. The magnitude of the piezocharge density also increases with the increasing tensile strain. Similar strain interrelated evolution trend of the piezocharge density can be found in the Ag-ZnO-Ag_polar tunnel junction.

Besides the overall evolution trend of the piezocharge density, there seems to be a subtile opposite evolution trend of the piezocharge densities on the left and right sides of each atomic layer. To verify it and investigate the quantitative dependence of the piezocharge on the applied strain, the total charge densities on the left and right sides of each atomic layer in the ZnO barrier are calculated under various strains. Here the total charge density on each side of each atomic layer is obtained by taking an integration of the planar average charge density distribution along the z direction in corresponding interval. Note that the calculated total charge density is closely related to the integral interval. From Figs. 2(a) and 2(c), we can observe the unartificial divisions (the peak and (or) the valley in the planar average potential energy) between adjacent atomic layers. Since the charge density is obtained basing on the potential energy by applying the Poisson's equation, these unartificial divisions are adopted to determine the integral interval in calculating the total charge density on each side of each atomic layer.

Fig. 7 shows the strain dependent total charge densities on the left and right sides of each Zn layer and O layer in the Ag-ZnO-Ag_zigzag tunnel junction. The left side and the right side of the nth A (A denotes Zn or O) atomic layer are labeled as nA_L and nA_R, respectively. The interfacial Zn and O layers are marked in the figure and the evolution trend of the total charge density is indicated by the solid line. It is found that, before applying external strain, the total charge densities on the left and right sides of each Zn layer or each O layer are not zero (i.e., not electrically neutral). It means that the charge distribution in the ZnO barrier is not uniform even in the tunnel junction with no strain. There are negative and positive total charge densities on the left and right sides of each Zn layer respectively in the Ag-ZnO-Ag_zigzag tunnel junction free of external strain. After applying external strain, all the Zn layers exhibit identical strain interrelated evolution trend of the total charge density. Both the total charge densities on the left and right sides of each Zn layer exhibit a decreasing tendency with the increasing compressive strain whereas an increasing tendency with the increasing tensile strain. At the same time, before applying external strain, the total charge densities on the left and right sides of each O layer in the Ag-ZnO-Ag_zigzag tunnel junction are positive and negative, respectively. Contrarily, after applying external strain, both the total charge densities on the left and right sides of each O layer increase with the increasing compressive strain whereas decrease with the increasing tensile strain. Basing on these strain interrelated evolution trends of the total charge density on each side of each atomic layer as well as the definition of piezocharge, the strain induced piezocharge profile of each Zn and O layers in the Ag-ZnO-Ag_zigzag tunnel junction can be derived and shown in Fig. 7(c). In the case of the c axis orientation of ZnO barrier pointing from right to left, there will be positive piezocharges emerging on the left sides of both the Zn and O layers and simultaneously negative piezocharges will emerge on their right sides when an in-plane compressive strain is applied to the ZnO barrier. Contrarily, after applying an in-plane tensile strain to the barrier, negative and positive piezocharges will respectively emerge on the left and right sides of both the Zn and O layers. Note that this is a factitious single atomic layer treatment method to intuitively perceive and apprehend the strain induced behavior of pizocharge. For the actual ZnO barrier, these emerging piezocharges on each side of each atomic layer are coherent together throughout the barrier and finally emerge at the terminated surfaces of the barrier. This reversible strain induced piezocharge is consistent with above strain dependent piezopotential energy, piezoelectric field and piezoelectric polarization (see the generalization in the following conclusion).

The strain dependent total charge densities on the left and right sides of each Zn and O layers in the Ag-ZnO-Ag_polar tunnel junction are also calculated as shown in Fig. 8. We can see that, besides the outmost atomic layers of ZnO barrier at the interfaces exhibit dissimilar behavior which may be due to the strong interaction between the ZnO barrier and the electrode at the interfaces,

the strain interrelated evolution trend of the total charge density on each side of the inner atomic layer in the Ag-ZnO-Ag_polar tunnel junction is identical with that in the Ag-ZnO-Ag_zigzag tunnel junction. Thus the derived piezocharge profile of the inner Zn and O layers under strain in the Ag-ZnO-Ag polar tunnel junction as show in Fig. 8(c) is also identical with that in the Ag-ZnO-Ag_zigzag tunnel junction, which also implies that this piezocharge is the intrinsic characteristic of the ZnO barrier.

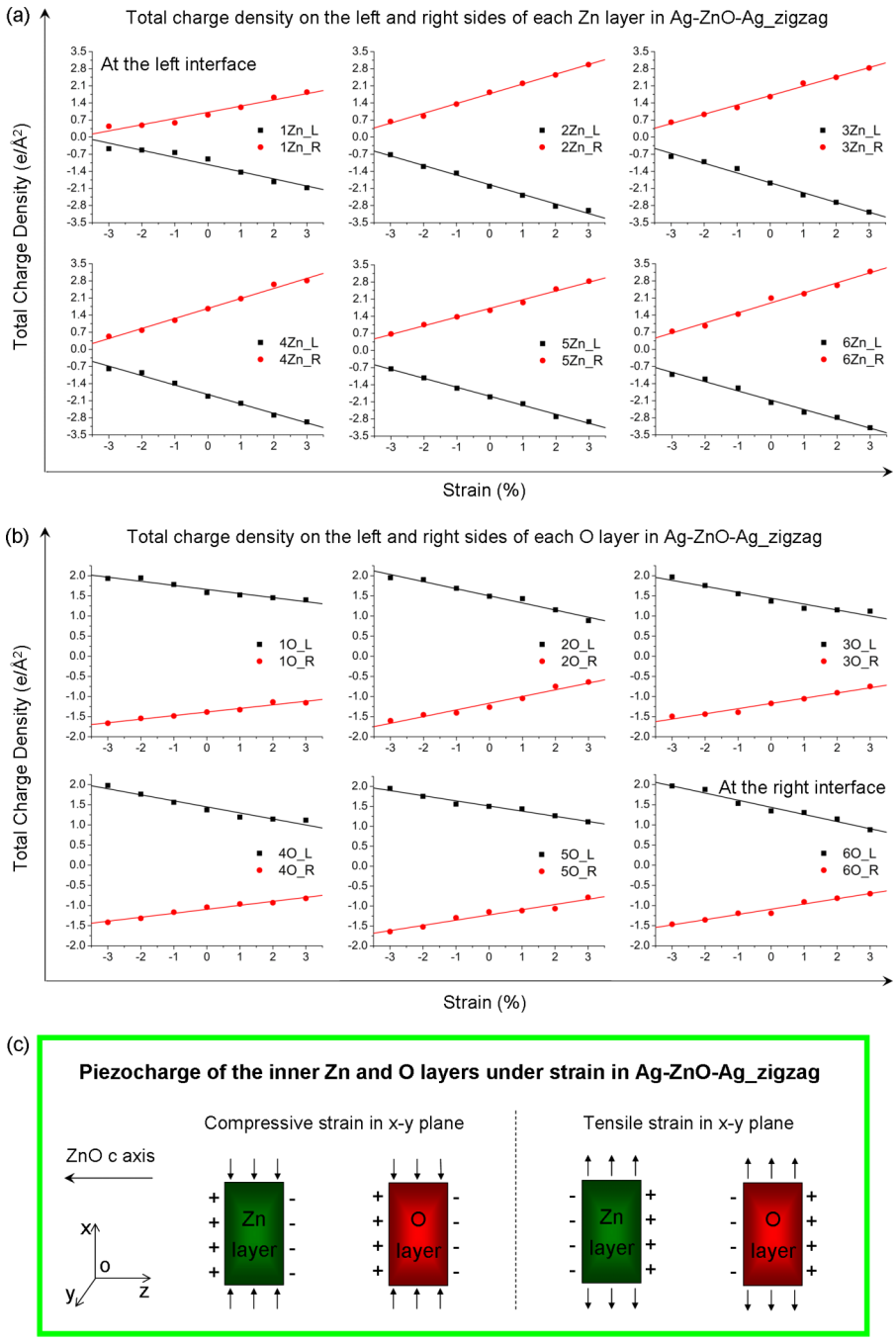

FIG. 7. Strain dependent total charge densities on the left and right sides of each Zn layer (a) and O layer (b) in the Ag-ZnO-Ag_zigzag tunnel junction. Specially, the interfacial Zn and O layers are marked and the evolution trend of the total charge density is indicated by the solid line. (c) The derived piezocharge profiles of the inner Zn and O layers under strain in the Ag-ZnO-Ag_zigzag tunnel junction.

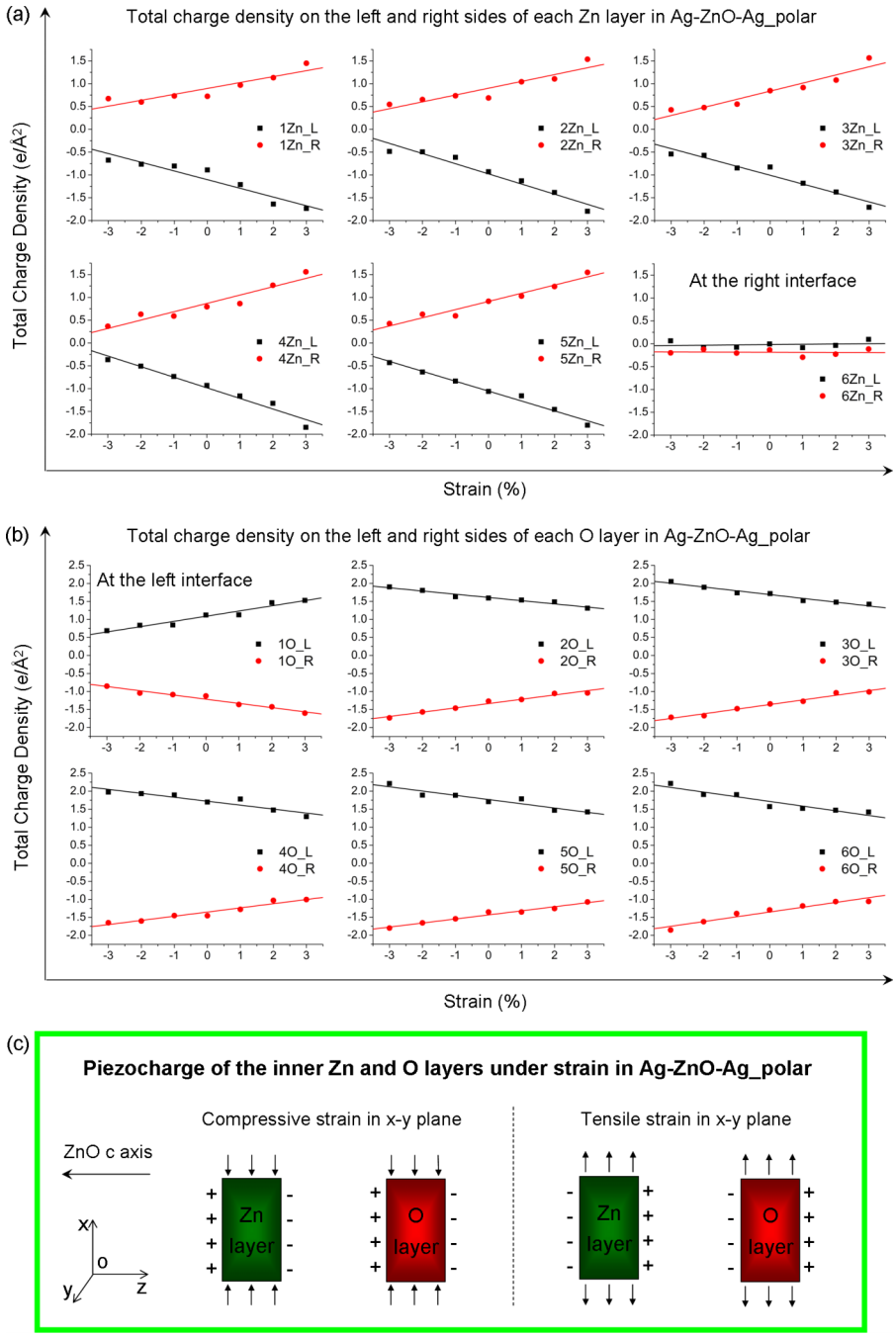

FIG. 8. Strain dependent total charge densities on the left and right sides of each Zn layer (a) and O layer (b) in the Ag-ZnO-Ag_polar tunnel junction. Specially, the interfacial Zn and O layers are marked and the evolution trend of the total charge density is indicated by the solid line. (c) The derived piezocharge profiles of the inner Zn and O layers under strain in the Ag-ZnO-Ag_polar tunnel junction.

IV. CONCLUSIONS

In summary, the embedded piezoelectricity (including the piezopotential energy, piezoelectric field, piezoelectric polarization and the piezocharge) and their correlation in two dissimilar Ag-ZnO-Ag piezoelectric tunnel junctions with different ZnO terminated surface structures are systematically investigated and explored basing on first principles quantum simulations. Results

show that all the studied physical quantities (i.e., the potential energy, built-in electric field, polarization and charge distribution) in the ZnO tunnel junction under strain can be considered as the composition of the structure based component and the reversible strain induced piezoelectric component. It is found that the directions of the non centrosymmetric structure based potential energy drop, built-in electric field and spontaneous polarization are consistent in each ZnO tunnel junction but opposite in the two ZnO tunnel junctions due to their different terminated surface structures. Meanwhile, the reversible strain induced piezopotential energy, piezoelectric field, piezoelectric polarization and piezocharge in the two ZnO tunnel junctions are identical since the ZnO c axes of these two tunnel junctions are in the same direction. Actually, they are verified to be the intrinsic characteristics of ZnO barrier basing on piezoelectric effect, which are independent of the system's structure but dependent on the c axis orientation of the ZnO barrier and the applied strain. As shown in Fig. 9, in the case of the c axis orientation of the ZnO barrier pointing from right to left, after applying an in-plane compressive strain to the barrier, positive and negative piezocharges will respectively emerge on the left and right sides of each Zn and O atomic layers and finally emerge at the left and right terminated surfaces of the ZnO barrier. Simultaneity, a piezopotential energy drop with negative and positive piezopotential energies emerging at the left and right terminated surfaces is induced throughout the ZnO barrier. Furthermore, a piezoelectric polarization pointing from right to left (in the same direction of the ZnO c axis) and a piezoelectric field (associated with the depolarization field) point from left to right are induced in the ZnO barrier. The magnitudes of all these piezoelectric physical quantities increase with the increasing compressive strain. When the

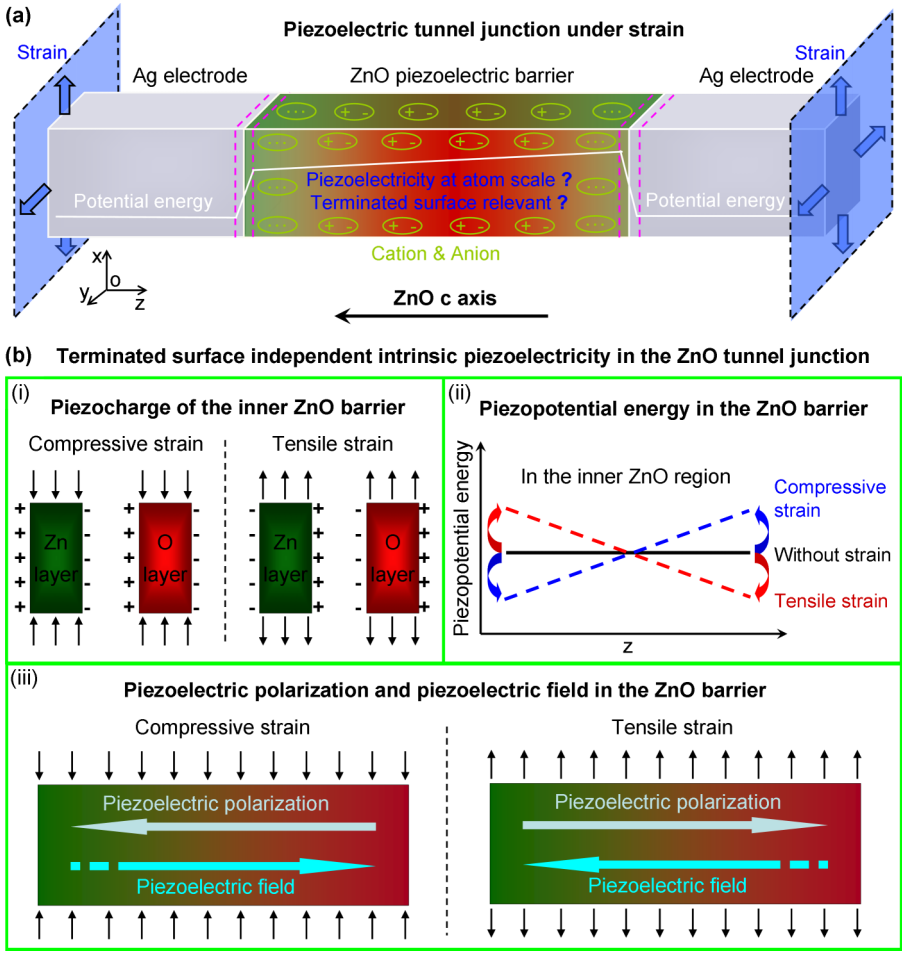

FIG. 9. The derived comprehensive picture of piezoelectricity in the ZnO tunnel junction, which is collected and summarized basing on Figs. 1-8.

applied strain switches from compressive to tensile, all these physical quantities would also reverse and increase with the increasing tensile strain. This revealed comprehensive picture of ZnO's piezoelectricity provides a quantitative perception on the piezoelectricity effect in the view of atomic scale quantum theory and may guide the further design of ZnO functional devices.

ACKNOWLEDGMENTS

The authors acknowledge the financial support of the China Postdoctoral Science Foundation (No. 2014M552267) and the National Natural Science Foundation of China (NSFC) (Nos. 11474363, 51172291, 11232015). Yue Zheng also thanks support from the Fundamental Research Funds for the Central Universities, New Century Excellent Talents in University, Research Fund for the Doctoral Program of Higher Education, Fok Ying Tung Foundation and Guangdong Natural Science Funds for Distinguished Young Scholar.

[1] W. Heywang, K. Lubitz, and W. Wersing, *Piezoelectricity: evolution and future of a technology* (Springer Science & Business Media, Heidelberg, 2008).
[2] R. S. Yang, Y. Qin, L. M. Dai, and Z. L. Wang, Nat. Nanotechnol. **4**, 34–39 (2009).
[3] J. Lee, W. Choi, Y. K. Yoo, K. S. Hwang, S. M. Lee, S. Kang, J. Kim, and J. H. Lee, Sensors **14**, 22199–22207 (2014).
[4] D. J. Shin, S. J. Jeong, C. E. Seo, K. H. Cho, and J. H. Koh, Ceram. Int. **41**, S686–S690 (2015).
[5] S. Nakamura, H. Numasato, K. Sato, M. Kobayashi, and I. Naniwa, Microsyst. Technol. **8**, 149–154 (2002).
[6] X. Chen, S. Y. Xu, N. Yao, and Y. Shi, Nano Lett. **10**, 2133–2137 (2010).
[7] Z. L. Wang, Adv. Func. Mater. **18**, 3553–3567 (2008).
[8] T. Zimmermann, M. Neuburger, P. Benkart, F. J. Hernández-Guillén, C. Pietzka, M. Kunze, I. Daumiller, A. Dadgar, A. Krost, and E. Kohn, IEEE Electr. Device Lett. **27**, 309–312 (2006).
[9] R. Agrawal and H. D. Espinosa, Nano Lett. **11**, 786–790 (2011).
[10] Y. F. Lin, J. H. Song, Y. Ding, S. Y. Lu, and Z. L. Wang, Appl. Phys. Lett. **92**, 022105 (2008).
[11] Z. L. Wang, J. Phys.: Condens. Matter **16**, R829–R858 (2004).
[12] Z. L. Wang, Nano Today **5**, 540–552 (2010).
[13] X. D. Wang, J. Zhou, J. H. Song, J. Liu, N. S. Xu, and Z. L. Wang, Nano Lett. **6**, 2768–2772 (2006).
[14] S. S. Kwon, W. K. Hong, G. Jo, J. Maeng, T. W. Kim, S. Song, and T. Lee, Adv. Mater. **20**, 4557–4562 (2008).
[15] A. Menzel, K. Subannajui, F. Güder, D. Moser, O. Paul, and M. Zacharias, Adv. Func. Mater. **21**, 4342–4348 (2011).
[16] Z. L. Wang, Mater. Today **10**, 20–28 (2007).
[17] J. H. He, P. H. Chang, C. Y. Chen, and K. T. Tsai, Nanotechnology **20**, 135701 (2009).
[18] Y. F. Gao and Z. L. Wang, Nano Lett. **9**, 1103–1110 (2009).
[19] Y. Zhang, Y. F. Hu, S. Xiang, and Z. L. Wang, Appl. Phys. Lett. **97**, 033509 (2010).
[20] Y. Zhang, Y. Liu, and Z. L. Wang, Adv. Mater. **23**, 3004–3013 (2011).
[21] B. Sen, M. Stroscio, and M. Dutta, J. Appl. Phys. **110**, 024506 (2011).
[22] M. T. Hoang, J. Yvonnet, A. Mitrushchenkov, and G. Chambaud, J. Appl. Phys. **113**, 014309 (2013).
[23] S. X. Dai, M. L. Dunn, and H. S. Park, Nanotechnology **21**, 445707 (2010).
[24] K. Momeni, G. M. Odegard, and R. S. Yassar, Acta Mater. **60**, 5117–5124 (2012).
[25] S. X. Dai and H. S. Park, J. Mech. Phys. Solids **61**, 385–397 (2013).
[26] G. H. Zhang, X. Luo, Y. Zheng, and B. Wang, Phys. Chem. Chem. Phys. **14**, 7051–7058 (2012).
[27] J. Zhu, W. J. Chen, G. H. Zhang, and Y. Zheng, Phys. Chem. Chem. Phys. **17**, 25583–25592 (2015).
[28] J. H. Lee, W. J. Lee, S. H. Lee, S. M. Kim, S. Kim, and H. M. Jang, Phys. Chem. Chem. Phys. **17**, 7857–7863 (2015).
[29] W. Liu, A. H. Zhang, Y. Zhang, and Z. L. Wang, Nano Energy **14**, 355–363 (2015).
[30] J. P. Perdew, K. Burke, and M. Ernzerhof, Phys. Rev. Lett. **77**, 3865–3868 (1996).
[31] G. Kresse and J. Furthmüller, Phys. Rev. B **54**, 11169–11186 (1996).
[32] G. Kresse and J. Hafner, Phys. Rev. B **48**, 13115–13118 (1993).
[33] P. E. Blöchl, Phys. Rev. B **50**, 17953–17979 (1994).
[34] H. J. Monkhorst and J. D. Pack, Phys. Rev. B **13**, 5188–5192 (1976).
[35] Y. F. Dong and L. J. Brillson, J. Electron. Mater. **37**, 743–748 (2008).
[36] T. Kamiya, K. Tajima, K. Nomura, H. Yanagi, and H. Hosono, Phys. Stat. Sol. A **205**, 1929–1933 (2008).
[37] L. Colombo, R. Resta, and S. Baroni, Phys. Rev. B **44**, 5572–5579 (1991).
[38] J. Junquera, M. H. Cohen, and K. M. Rabe, J. Phys.: Condens. Matter **19**, 213203 (2007).
[39] G. H. Zhang, Y. Zheng, and B. Wang, J. Appl. Phys. **114**, 044111 (2013).
[40] X. Gonze and C. Lee, Phys. Rev. B **55**, 10355–10368 (1997).
[41] X. F. Wu, D. Vanderbilt, and D. R. Hamann, Phys. Rev. B **72**, 035105 (2005).
[42] C. Q. Qin, Y. S. Gu, X. Sun, X. Q. Wang, and Y. Zhang, Nano Res. **8**, 2073-2081 (2015).